


RESEARCH ARTICLE | OCTOBER 14 2024

Vibrational squeezing via spin inversion pulses

Marc-Dominik Krass ; Nils Prumbaum  ; Raphael Pachlatko; Christian L. Degen ; Alexander Eichler 



Appl. Phys. Lett. 125, 164101 (2024)

<https://doi.org/10.1063/5.0233135>



Articles You May Be Interested In

Adaptive control of force microscope cantilever dynamics

J. Appl. Phys. (September 2007)

Feasibility of imaging in nuclear magnetic resonance force microscopy using Boltzmann polarization

J. Appl. Phys. (February 2019)

Magnetic resonance force microscopy

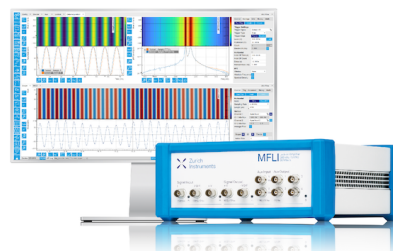
Physics Today (June 2007)

Challenge us.

What are your needs for periodic signal detection?



Find out more



Vibrational squeezing via spin inversion pulses

Cite as: Appl. Phys. Lett. **125**, 164101 (2024); doi: [10.1063/5.0233135](https://doi.org/10.1063/5.0233135)

Submitted: 12 August 2024 · Accepted: 3 October 2024 ·

Published Online: 14 October 2024



View Online



Export Citation



CrossMark

Marc-Dominik Krass,^{a)}  Nils Prumbaum,^{b)}  Raphael Pachlatko,^{c)}  Christian L. Degen,^{c)}  and Alexander Eichler 

AFFILIATIONS

Laboratory for Solid State Physics, ETH Zürich, CH-8093 Zürich, Switzerland

^{a)}Present address: attocube systems AG, DE-85540 Haar, Germany.

^{b)}Author to whom correspondence should be addressed: nilspr@phys.ethz.ch

^{c)}Present address: QUAD Systems AG, CH-8305 Dietlikon, Switzerland.

ABSTRACT

Magnetic resonance force microscopy (MRFM) describes a range of approaches to detect nuclear spins with mechanical sensors. MRFM has the potential to enable magnetic resonance imaging with near-atomic spatial resolution, opening up exciting possibilities in solid state and biological research. In many cases, the spin-mechanics coupling in MRFM is engineered with the help of periodic radio frequency pulses. In this paper, we report that such pulses can result in unwanted parametric amplification of the mechanical vibrations, causing misinterpretation of the measured signal. We show how the parametric effect can be canceled by auxiliary radio frequency pulses or by appropriate post-correction after careful calibration. Future MRFM measurements may even make use of the parametric amplification to reduce the impact of amplifier noise.

© 2024 Author(s). All article content, except where otherwise noted, is licensed under a Creative Commons Attribution (CC BY) license (<https://creativecommons.org/licenses/by/4.0/>). <https://doi.org/10.1063/5.0233135>

Nanomechanical sensors are excellent devices for spin detection and provide the basis for several ambitious proposals in quantum transduction and nanoscale imaging. On the one hand, spin-mechanics coupling is envisioned to enable readout and transfer of the polarization states of individual spins.¹ The realization of this proposal would allow quantum information exchange between remote spin qubits. On the other hand, spin-mechanics coupling also forms the basis of magnetic resonance force microscopy (MRFM),^{2–5} which could become a transformative technology for nondestructive imaging of individual, complex biomolecules. While current proof-of-principle demonstrations are still too coarse-grained to reveal interesting structural information,^{6–8} the method will profit greatly from the progress achieved with optomechanical systems, and especially with high-Q silicon nitride resonators.^{9–15}

Typical spin-mechanics experiments rely on a non-resonant, weak coupling between the spins in a sample and the mechanical sensor, mediated by a magnetic field gradient. Non-resonant coupling signifies that the resonance frequency f_0 of the sensor is much lower than the Larmor frequency $f_L = \gamma B / 2\pi$ of spins, where γ is the gyromagnetic ratio and B an applied magnetic field strength. In order to engineer efficient coupling between the spins and the sensor, a number of different protocols have been developed.^{16–19} A commonly used method relies on pulsed radio frequency (rf) magnetic fields to periodically invert the spins.^{6,7} With a pulse repetition rate of $2f_0$, the

interaction between the spins and a magnetic field gradient generates a force at f_0 that drives the sensor into measurable oscillations.

Most MRFM setups operate in the weak-coupling regime, where the averaging time required to pickup a spin signal is much longer than the effective spin lifetime in the rotating frame τ_m .^{20–22} In addition, the thermal spin polarization is negligible for small spin ensembles. As a consequence, the relevant measured quantity is not the instantaneous oscillation amplitude, which reflects the instantaneous spin ensemble polarization. Instead, the stochastic fluctuations of the spin ensemble over times $t \gg \tau_m$ lead to a force noise that increases the variance of the sensor's oscillation.^{20,23} The resulting sensor fluctuations in phase space still have a Gaussian distribution in both quadratures (X and Y), but one of the quadratures shows an increase in the variance.

In this paper, we reveal that the pulsed spin inversion method can produce a spurious driving effect that manifests as an increase in the sensor oscillation variance in one quadrature. This effect, while observed and heuristically avoided in the past, is little understood. The spurious driving closely resembles a real spin signal and can, therefore, lead to misinterpretation of data. We propose that the observed effect is due to phase-dependent parametric amplification (squeezing) of the sensor's thermomechanical fluctuations. We demonstrate that the squeezing artifact can be suppressed by the addition of a second set of pulses between the spin inversion pulses, which “unsqueezes” the

phase space distribution. In this way, we are able to obtain an artifact-free spin signal.

In our setup, the fundamental mode of a silicon cantilever acts as the mechanical sensor. The cantilever is positioned in the pendulum geometry above a gold microstrip fabricated on top of a thermally oxidized silicon chip. The cantilever has a resonance frequency $f_0 = 3500$ Hz, an effective mass $m = 10^{-13}$ kg, and a quality factor $Q = 25\,000$. The ringdown time of the cantilever is reduced to $\tau = 20$ ms via a feedback-cooling technique.²⁴ For spin-mechanics experiments, a sample is attached to the tip of the cantilever, which is cooled down to $T \approx 5$ K. The spin ensemble inside the sample, which is the typical subject of study in MRFM, is illustrated by a single blue spin in Fig. 1(a).

In order to manipulate the spin ensemble, amplitude-modulated rf current pulses swept over a frequency window around f_L are sent through the microstrip on the chip surface.⁷ The current generates rf magnetic fields that flip spins once every pulse, see top window in Fig. 1(b). With a pulse repetition rate of $2f_0$, the interaction of the z -component of the spin ensemble I_z with the magnetic field gradient of a nanoscale ferromagnet [Fig. 1(a)] creates a periodic force that drives the cantilever oscillation at f_0 . Stochastic spin fluctuations with lifetime $\tau_m \approx 40$ ms slowly change I_z and average the mean force signal to zero over long integration times $t \gg \tau_m$. For this reason, it is usually the added oscillation variance σ_{spin}^2 caused by the fluctuating spin force that serves as the spin signal in MRFM.^{20,23} By selecting the pulse phase relative to the lock-in amplifier clock at f_0 , the phase of σ_{spin}^2 can be controlled; in the example shown in Fig. 1(c), the spin signal is chosen to be in the X channel. The spin force manifests as a difference between the variances in the two quadratures, $\sigma_{\text{spin}}^2 = \sigma_X^2 - \sigma_Y^2$. Note that the pulses at $2f_0$ do not cause direct electrostatic driving of the cantilever

mode at f_0 because they do not break the symmetry over one period $T_c = 1/f_0$.

Surprisingly, a significant imbalance between σ_X^2 and σ_Y^2 can be observed experimentally even when spin inversions are suppressed. This is done by either detuning the window of Larmor frequencies that are addressed by the pulse, or by reducing the window size to zero.⁷ In such a situation, one would expect that the pulses have no effect on the cantilever mode and that the phase space portrait of the thermal fluctuations remains circular as in Fig. 2(a). Instead, we clearly observe a significant imbalance $\sigma_X^2 > \sigma_Y^2$ in Fig. 2(b). This imbalance could be misinterpreted as a spin signal. When the phase of the pulse is rotated by 90° [Fig. 1(d)], the resulting variance is rotated as well, yielding $\sigma_Y^2 > \sigma_X^2$ in Fig. 2(c). When combining both sets of pulses (0° and 90°), we return to a balanced distribution $\sigma_X^2 \approx \sigma_Y^2$, see Fig. 2(d). Here, both quadratures are slightly enlarged relative to Fig. 2(a), indicating an increase in the effective cantilever mode temperature.

To understand the observations in Fig. 2, we need to consider two independent effects. On the one hand, current pulses dissipate energy, heating the cantilever mode irrespective of the pulse shape or phase. We assign the increase in σ_X^2 and σ_Y^2 , which is most clearly visible in Fig. 2(d) relative to Fig. 2(a), yet also present in Figs. 2(b) and 2(c), to such Joule heating. On the other hand, we observe that the average squared voltage $\langle U^2 \rangle$ applied to the microstrip can modify the cantilever spring constant k (and the resonance frequency f_0) in a roughly linear manner, see Fig. 3. We tentatively associate this effect with an electrostatic force $F_e \propto Uq_i$ between the surface bias U and charges q_i on the cantilever tip.^{25,26} When the charges are induced by the voltage itself as $q_i \propto U$, this effect becomes quadratic in voltage as $F_e \propto U^2$,²⁷ similar to the tuning effect observed in carbon nanotube resonators.²⁸ However, we cannot rule out models based on time-dependent

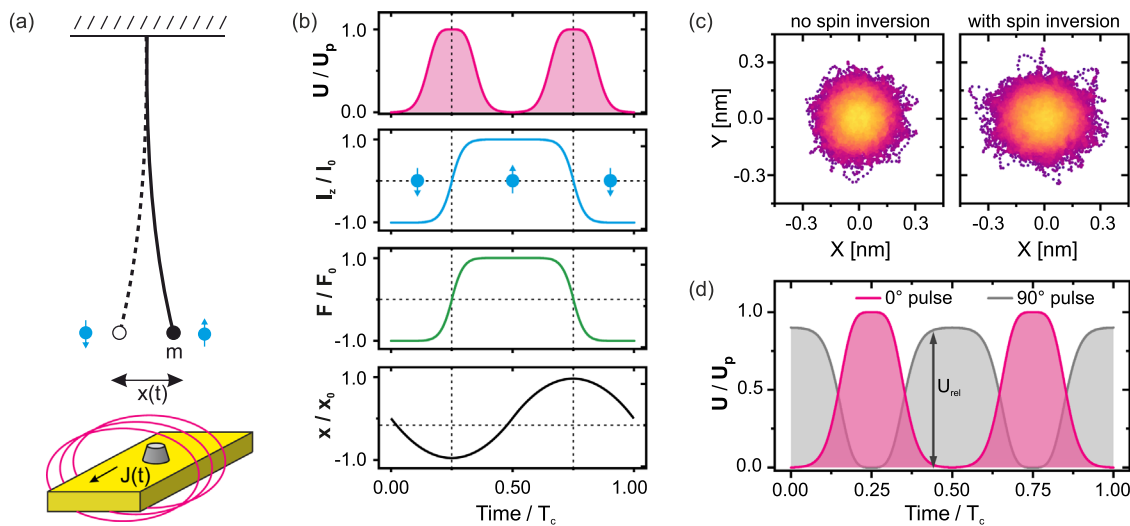


FIG. 1. Nanomechanical spin detection protocol. (a) Illustration of the MRFM setup comprising a spin ensemble (blue arrow) at the tip of a cantilever sensor with mass m . A pulsed current $J(t)$ through a microstrip produces a magnetic field (pink lines) that periodically inverts the spin ensemble polarization I_z . The interaction between I_z and a magnetic field gradient from a nanomagnet (grey cone) creates a force F that drives cantilever oscillations $x(t)$. (b) Timing diagram of pulse voltage U (with peak voltage U_p), spin polarization I_z (with maximum value I_0), force F (with amplitude F_0), and cantilever displacement x (with amplitude x_0) over one cantilever period T_c . (c) Measured fluctuations of the cantilever oscillations in a phase space rotating at f_0 without and with spin inversion over a measurement time of $t = 180$ s. The quadratures are defined as $x(t) = X(t) \cos(2\pi f_0 t) - Y(t) \sin(2\pi f_0 t)$, with a slowly changing amplitude $x_0 = \sqrt{X^2 + Y^2}$. The color code indicates probability density from low (pink) to high (yellow). The fluctuating spin force manifests as an increased variance σ_X^2 . (d) Amplitude modulation of 0° pulses and 90° pulses, with relative amplitude U_{rel} .

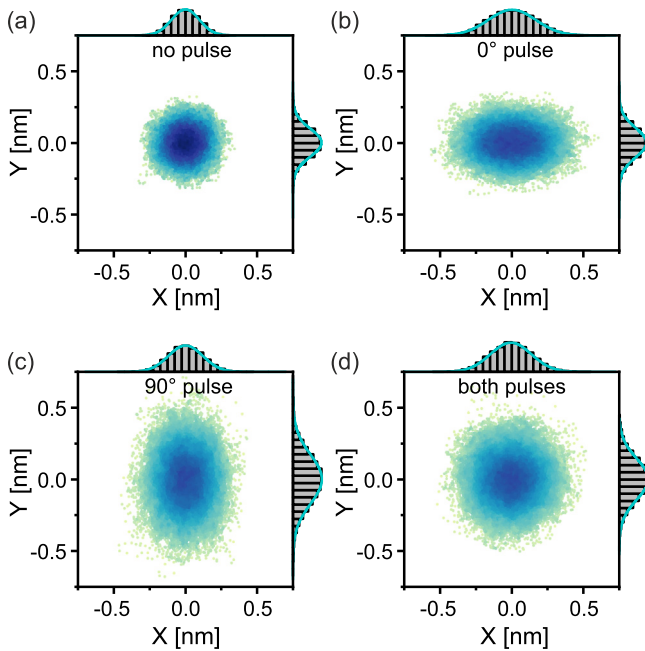


FIG. 2. Fluctuations measured while spin inversions are suppressed, with $t = 240$ s. The color code indicates probability density from low (yellow) to high (dark blue). Histograms quantify the distributions in X and Y in phase space. (a) Thermomechanical noise of the cantilever mode when no pulses are applied. The widths of the Gaussian fits correspond to $\sigma_X = 96.5$ pm and $\sigma_Y = 97.9$ pm. (b) Fluctuations in the presence of 0° pulses, with $\sigma_X = 164.8$ pm and $\sigma_Y = 103.1$ pm. (c) Fluctuations in the presence of 90° pulses, with $\sigma_X = 119.8$ pm and $\sigma_Y = 172.6$ pm. (d) Fluctuations in the presence of both 0° and 90° pulses, with $\sigma_X = 142.4$ pm and $\sigma_Y = 143.2$ pm.

Joule heating and associated length contractions. In either case, when the field power is modulated in time with a rate close to $2f_0$, it causes positive and negative parametric amplification of the orthogonal oscillation quadratures.^{29–31} As the amplification is far below the threshold for parametric oscillation, no spontaneous time-translation symmetry breaking occurs.³² However, the phase space portrait of the resonator

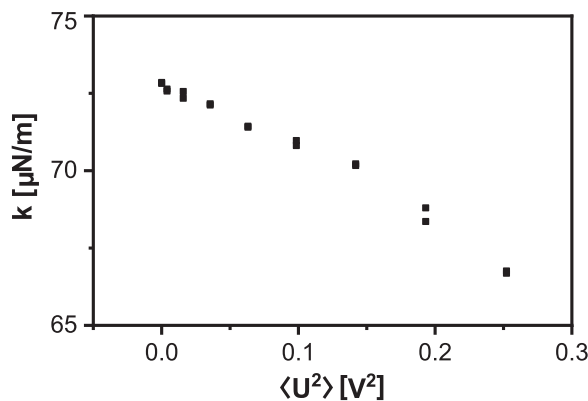


FIG. 3. Spring constant ($k = 4\pi^2 m f_0^2$) of the cantilever mode measured as a function of average pulse power $\langle U^2 \rangle$. We observe a roughly linear decrease in k with $\langle U^2 \rangle$.

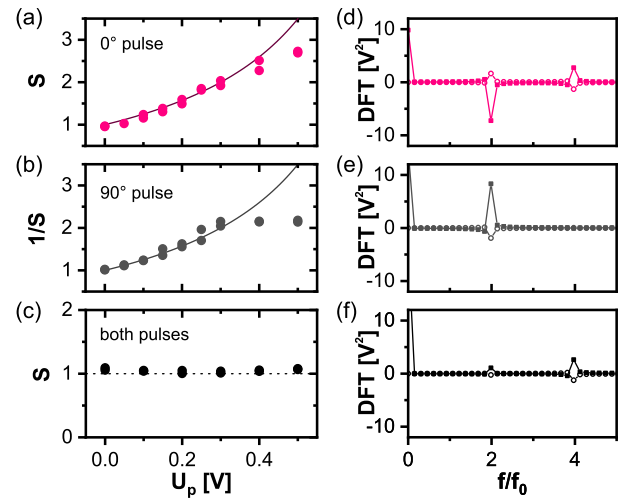


FIG. 4. (a) Squeezing factor $S = \sigma_X^2 / \sigma_Y^2$ as a function of the pulse amplitude U_p for 0° pulses applied to the cantilever. A line quantifies the expected trend, see main text. This trend describes the data well up to $U_p \approx 0.4$ V, beyond which we found instabilities in our pulse generation setup. (b) Same as in (a) but for 90° pulses, showing $1/S$ instead of S . (c) Squeezing factor when both pulses are applied simultaneously. A dashed line at $S = 1$ is a guide to the eye. (d)–(f) Discrete Fourier transforms (DFT) of the measured pulse shapes used in (a)–(c), respectively. Real and imaginary components of the DFT are shown as filled squares and open spheres, respectively. We find that the DFTs have positive, negative, and vanishing amplitudes at $f/f_0 = \pm 2$ for the three respective situations.

is squeezed, i.e., X and Y experience positive and negative amplification, respectively.

To show that parametric amplification can be used to model our experimental observations, we examine the measured squeezing factor $S = \sigma_X^2 / \sigma_Y^2$ in Fig. 4. When only the 0° rf pulses are applied (without inverting any spins), S increases monotonically with the maximum pulse amplitude U_p . In contrast, when only the rotated 90° pulses are used, the inverse $1/S$ increases monotonically with U_p . Both findings are in agreement with the observations in Fig. 2. Beyond $U_p \approx 0.4$ V, the squeezing saturates for both pulse types. In this voltage regime, we found spurious effects in our pulse protocol that may cause further artifacts. We avoid this voltage range in our MRFM experiments and also ignore it in the following discussion.

To quantify the changes in S , we plot in Figs. 4(a) and 4(b) the expected parametric squeezing ratio $(1 + \beta U_p) / (1 - \beta U_p)$ ³⁰ as solid lines, where $\beta = 1.11 \text{ V}^{-1}$ is a heuristic factor to account for the interaction efficiency between the pulses and the cantilever displacement. This simple model accounts well for the observed increase in S and $1/S$, respectively, in the relevant range $U_p < 0.4$ V. When parametric amplification is applied to both quadratures simultaneously, symmetry between fluctuations in X and Y should be restored. Indeed, in Fig. 4(c) we show that $S \approx 1$ when both 0° and 90° are combined. This entails that 90° pulses can be used to counter unwanted squeezing during spin detection measurements. In the past, this spurious driving was avoided by heuristic pulse optimization without full knowledge of the mechanism described in this Letter.^{7,8,33–35}

The origin of the parametric squeezing, and its cancellation by the combination of 0° and 90° pulses, can be confirmed by a Fourier analysis of the applied pulse shapes. In Fig. 4(d), we display the discrete

Fourier transform (DFT) of the measured squared pulse voltage (the pulse power) for the 0° pulse. The spectrum has a peak at $2f_0$, as expected from the amplitude modulation of the pulse, as depicted in Fig. 1(d). This Fourier component at $2f_0$ is responsible for parametric amplification and squeezing of the cantilever oscillations. We obtain the same result for the 90° pulse in Fig. 4(e). However, the sign of the component at $2f_0$ is inverted, as expected for the DFT of a squared and $\pi/2$ phase-shifted sinusoidal signal. Finally, when both pulses are combined, the positive and negative peaks of the pulses cancel and the resulting spectrum has almost no signature near $2f_0$. As a consequence, no parametric squeezing effects are present.

Our understanding of the parametric amplification effect can be used to efficiently cancel the spurious driving in the presence of a spin signal by applying compensation pulses shifted by 90° relative to the spin inversion pulses. Note that the 0° and 90° pulses can have different amplitude modulation functions and peak amplitudes, cf. Fig. 1(d). As long as the $2f_0$ -component of both pulses is equal in magnitude, the parametric squeezing is compensated. This enables significant freedom in optimizing spin inversion protocols. To find a suitable compensation pulse, we perform the following calibration measurement: first, a spin inversion 0° pulse is selected, but modified such that spin inversions are suppressed (see above). Thus, the pulse generates a spurious driving effect that is identical to that in a spin measurement. The optimal 90° compensation pulse is then chosen by minimizing the quadrature mismatch $\sigma_{\text{spur}}^2 = \sigma_x^2 - \sigma_y^2$. Finally, the spin inversion pulse parameters are switched back to enable spin sensing. In this way the measured imbalance σ_{spin}^2 stems from the spin force, not from spurious driving. The measurements presented in Fig. 1(c) were obtained using this compensation pulse calibration: the left panel shows data measured with a non-spin-inverting 0° pulse, while the right uses a spin-inverting 0° pulse with identical amplitude modulation.

In summary, we reveal that spin inversion pulses in MRFM can result in the parametric squeezing of cantilever vibrations, which yields a signal that closely resembles that of a real spin force. The effect can be canceled by combining two sets of phase-shifted pulses: the 0° pulses are applied at a carrier frequency f_L to invert nuclear spins within a selected Larmor frequency band, while the 90° pulse are detuned from f_L and do not excite spins. This method is very robust: once a suitable 90° pulse is found, the compensation works regardless of the instantaneous cantilever frequency or the pulse amplitude scaling, which is very beneficial for scanning experiments. A disadvantage of adding the 90° pulses is increased Joule heating, as shown in Fig. 2(d). For this reason, it is worth considering alternative methods for reducing the squeezing effect of the 0° pulses.

With a careful calibration of the parametric interaction, the squeezing can be removed from the collected spin force data in post analysis by applying the inverse function $(1 - \beta U_p)/(1 + \beta U_p)$, where the value of β can be obtained from a measurement series as shown in Fig. 4(a). With this method, no second pulse is required to cancel the resonator oscillation squeezing, and hence Joule heating is reduced. Squeezing can potentially even turn into a resource for enhancing the spin signal relative to amplifier noise, leading to an enhanced signal-to-noise ratio. However, note that the ratio between the measured spin force and force fluctuations acting on the sensor is not changed by squeezing, hence no sensitivity increase relative to the dominant thermomechanical force noise is expected.

We expect that the understanding of parametric effects related to spin driving will enable researchers to design better pulse shapes via optimal control theory³⁶ and machine learning, thereby leading to improved spin sensing protocols. Such design rules will be crucial for establishing spin sensing protocols with mechanical sensors in the MHz regime. These are expected to improve spin sensitivity, but come with the need for much faster nuclear spin manipulations.^{15,19,37,38}

We thank the operations team of the FIRST cleanroom, especially Sandro Loosli and Petra Burkard, as well as the operations team of the Binnig and Rohrer Nanotechnology Center (BRNC) at IBM R schlikon, especially Ute Drechsler, Richard Stutz, and Dr. Diana D vila Pineda. A. E. acknowledges financial support from the Swiss National Science Foundation (SNSF) through Grant Nos. 200021_200412 and CRSII5_206008/1.

AUTHOR DECLARATIONS

Conflict of Interest

The authors have no conflicts to disclose.

Author Contributions

Marc-Dominik Krass and Nils Prumbaum contributed equally to this work.

Marc-Dominik Krass: Conceptualization (equal); Formal analysis (equal); Investigation (equal); Writing – review & editing (equal). **Nils Prumbaum:** Data curation (equal); Investigation (equal); Writing – original draft (equal). **Raphael Pachlatko:** Data curation (equal); Writing – review & editing (equal). **Christian L. Degen:** Resources (equal); Supervision (equal); Writing – review & editing (equal). **Alexander Eichler:** Resources (equal); Supervision (equal); Writing – original draft (equal).

DATA AVAILABILITY

The data that support the findings of this study are available from the corresponding author upon reasonable request.

REFERENCES

- ¹P. Rabl, S. J. Kolkowitz, F. Koppens, J. Harris, P. Zoller, and M. D. Lukin, *Nat. Phys.* **6**, 602 (2010).
- ²J. A. Sidles, *Appl. Phys. Lett.* **58**, 2854 (1991).
- ³J. A. Sidles, J. L. Garbini, and G. P. Drobny, *Rev. Sci. Instrum.* **63**, 3881 (1992).
- ⁴D. Rugar, C. Yannoni, and J. Sidles, *Nature* **360**, 563 (1992).
- ⁵M. Poggio and C. L. Degen, *Nanotechnology* **21**, 342001 (2010).
- ⁶C. Degen, M. Poggio, H. Mamin, C. Rettner, and D. Rugar, *Proc. Natl. Acad. Sci. U. S. A.* **106**, 1313 (2009).
- ⁷U. Grob, M. D. Krass, M. H ritier, R. Pachlatko, J. Rhensius, J. Ko ata, B. A. Moores, H. Takahashi, A. Eichler, and C. L. Degen, *Nano Lett.* **19**, 7935 (2019).
- ⁸M.-D. Krass, N. Prumbaum, R. Pachlatko, U. Grob, H. Takahashi, Y. Yamauchi, C. L. Degen, and A. Eichler, *Phys. Rev. Appl.* **18**, 034052 (2022).
- ⁹Y. Tsaturyan, A. Barg, E. S. Polzik, and A. Schliesser, *Nat. Nanotechnol.* **12**, 776 (2017).
- ¹⁰C. Reetz, R. Fischer, G. Assump o, D. McNally, P. Burns, J. Sankey, and C. Regal, *Phys. Rev. Appl.* **12**, 044027 (2019).
- ¹¹A. H. Ghadimi, S. A. Fedorov, N. J. Engelsens, M. J. Beryhi, R. Schilling, D. J. Wilson, and T. J. Kippenberg, *Science* **360**, 764 (2018).
- ¹²T. Gisler, M. Helal, D. Sabonis, U. Grob, M. H ritier, C. L. Degen, A. H. Ghadimi, and A. Eichler, *Phys. Rev. Lett.* **129**, 104301 (2022).

- ¹³M. J. Beryhi, A. Arabmoheghi, A. Beccari, S. A. Fedorov, G. Huang, T. J. Kippenberg, and N. J. Engels, *Phys. Rev. X* **12**, 021036 (2022).
- ¹⁴D. Shin, A. Cupertino, M. H. J. de Jong, P. G. Steeneken, M. A. Bessa, and R. A. Norte, *Adv. Mater.* **34**, 2106248 (2022).
- ¹⁵A. Eichler, *Mater. Quantum Technol.* **2**, 043001 (2022).
- ¹⁶J. M. Nichol, T. R. Naibert, E. R. Hemesath, L. J. Lauhon, and R. Budakian, *Phys. Rev. X* **3**, 031016 (2013).
- ¹⁷H. Mamin, M. Poggio, C. Degen, and D. Rugar, *Nat. Nanotechnol.* **2**, 301 (2007).
- ¹⁸A. Vinante, G. Wijts, O. Usenko, L. Schinkelshoek, and T. Oosterkamp, *Nat. Commun.* **2**, 572 (2011).
- ¹⁹J. Kořata, O. Zilberberg, C. L. Degen, R. Chitra, and A. Eichler, *Phys. Rev. Appl.* **14**, 014042 (2020).
- ²⁰C. L. Degen, M. Poggio, H. J. Mamin, and D. Rugar, *Phys. Rev. Lett.* **99**, 250601 (2007).
- ²¹C. L. Degen, M. Poggio, H. J. Mamin, and D. Rugar, *Phys. Rev. Lett.* **100**, 137601 (2008).
- ²²C. P. Slichter, *Principles of Magnetic Resonance* (Springer Science & Business Media, 2013), Vol. 1.
- ²³B. Herzog, D. Cadecdu, F. Xue, P. Peddibhotla, and M. Poggio, *Appl. Phys. Lett.* **105**, 043112 (2014).
- ²⁴M. Poggio, C. L. Degen, H. J. Mamin, and D. Rugar, *Phys. Rev. Lett.* **99**, 017201 (2007).
- ²⁵S. M. Yazdani, J. A. Marohn, and R. F. Loring, *J. Chem. Phys.* **128**, 224706 (2008).
- ²⁶M. Héritier, R. Pachlatko, Y. Tao, J. M. Abendroth, C. L. Degen, and A. Eichler, *Phys. Rev. Lett.* **127**, 216101 (2021).
- ²⁷S. M. Yazdani, N. Hoepker, S. Kuehn, R. F. Loring, and J. A. Marohn, *Nano Lett.* **9**, 2273 (2009).
- ²⁸V. Sazonova, Y. Yaish, H. Üstünel, D. Roundy, T. A. Arias, and P. L. McEuen, *Nature* **431**, 284 (2004).
- ²⁹D. Rugar and P. Grütter, *Phys. Rev. Lett.* **67**, 699 (1991).
- ³⁰M. C. Lifshitz and R. Cross, “Nonlinear dynamics of nanomechanical and micromechanical resonators,” in *Reviews of Nonlinear Dynamics and Complexity* (Wiley-VCH, 2009), pp. 1–52.
- ³¹A. Eichler and O. Zilberberg, *Classical and Quantum Parametric Phenomena* (Oxford University Press, 2023).
- ³²M. I. Dykman, C. M. Maloney, V. N. Smelyanskiy, and M. Silverstein, *Phys. Rev. E* **57**, 5202 (1998).
- ³³J. G. Longenecker, H. Mamin, A. W. Senko, L. Chen, C. T. Rettner, D. Rugar, and J. A. Marohn, *ACS Nano* **6**, 9637 (2012).
- ³⁴B. Moores, A. Eichler, Y. Tao, H. Takahashi, P. Navaretti, and C. L. Degen, *Appl. Phys. Lett.* **106**, 213101 (2015).
- ³⁵R. Pachlatko, N. Prumbaum, M.-D. Krass, U. Grob, C. L. Degen, and A. Eichler, *Nano Lett.* **24**, 2081 (2024).
- ³⁶W. Rose, H. Haas, A. Q. Chen, N. Jeon, L. J. Lauhon, D. G. Cory, and R. Budakian, *Phys. Rev. X* **8**, 011030 (2018).
- ³⁷H. Haas, S. Tabatabaei, W. Rose, P. Sahafi, M. Piscitelli, A. Jordan, P. Priyadarsi, N. Singh, B. Yager, P. J. Poole *et al.*, *Proc. Natl. Acad. Sci.* **119**, e2209213119 (2022).
- ³⁸S. Tabatabaei, P. Priyadarsi, N. Singh, P. Sahafi, D. Tay, A. Jordan, and R. Budakian, *arXiv:2402.16283* (2024).